Supplementary Material
Progressive Divide-and-Conquer via Subsampling Decomposition for Accelerated MRI

Chong Wang, Lanqing Guo, Yufei Wang, Hao Cheng, Yi Yu, Bihan Wen*
Nanyang Technological University, Singapore
{wang1711, lanqing001, yufei001, HAO006, yuyi0010, bihan.wen}@ntu.edu.sg

In this supplementary material, we include more implementation details of the architecture of the proposed degradation predictor (Section A) and the severity conditioning module (Section B). Besides, we provide a visualization of each intermediate result in PDAC iterations in Section C and more visual examples on multi-coil reconstruction on fastMRI knee and Stanford2D FSE datasets in Section D.

A. Architecture of Degradation Predictor

During each iteration of PDAC, we learn the decomposed degradation as an auxiliary task along the reconstruction process. In the context of accelerated MRI, this decomposed degradation corresponds to the Cartesian sampling mask M_t on the k-space, which could be simply represented using a binary vector $\boldsymbol{m}_t$. Specifically, we introduce a degradation predictor $\mathcal{P}_{\theta_t}$ to estimate a probability vector $\boldsymbol{p}_t \in \mathbb{R}^{1\times d}$ indicating the reconstruction confidence on each frequency column in the current recovered k-space $\tilde{Z}_t \in \mathbb{C}^{C\times H\times W}, d = W$. The detailed architecture of $\mathcal{P}_{\theta_t}$ is illustrated in Figure A. Consequently, $\boldsymbol{m}_t$ can be obtained by adding extra support, indicating the location of frequency columns to preserve, on the previous mask $\boldsymbol{m}_{t-1}$. Such support is selected from the indices of several top largest values in $\boldsymbol{p}_t$.

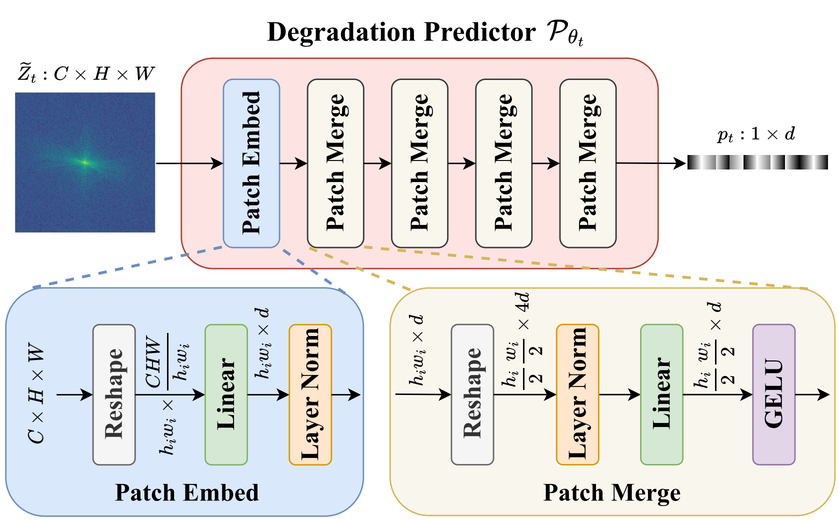

Figure A. The detailed architecture of the proposed degradation predictor $\mathcal{P}_{\theta_t}$. It estimates the probability $\boldsymbol{p}_t$ indicating the confidence on each frequency column in the reconstruction $\tilde{Z}_t$.

*Corresponding author: Bihan Wen.

B. Architecture of Severity Conditioning Module

During each iteration in PDAC, the network input $\boldsymbol{z}_{t-1}$ suffers from a specific degradation pattern in the k-space which is characterized by M_{t-1}. Therefore, we propose to integrate such information on the degradation severity indicated by $\boldsymbol{m}_{t-1}$ together with the previous probability vector $\boldsymbol{p}_t$ using a severity conditioning module E_{θ_t}. The detailed architecture of E_{θ_t} is shown in Figure B, where the information of masked probability $\boldsymbol{m}_{t-1} \odot \boldsymbol{p}_{t-1}$ is embedded via the adaptive layer norm (adaLN) [2] into the network.

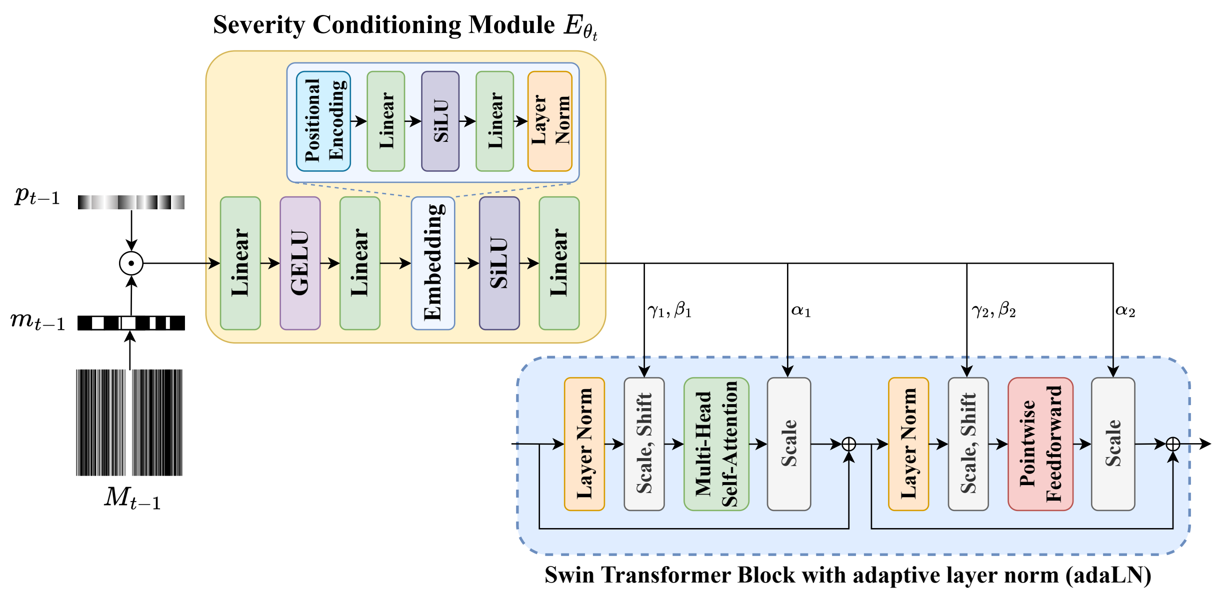

Figure B. The detailed architecture of the proposed severity conditioning module E_{θ_t}. It integrates the information in the masked confidence $\boldsymbol{m}_t \odot \boldsymbol{p}_t$ via adaptive layer norm (adaLN) into the Swin transformer blocks [2].

C. Visualization of Progressive Reconstruction

Figure C demonstrates the each intermediate results of decomposed degradation M_t, reconstructed k-space $\boldsymbol{z}_t$ and reconstructed MR images $\boldsymbol{x}_t$, respectively, with total iteration $T = 8$. With the merit of the proposed progressive divide-and-conquer, each iteration in PDAC selectively retrieves information within specific segments of the null space. The information in the k-space is restored progressively from low frequencies, which is easier to recover, to more challenging high frequencies, as shown in the second row in Figure C. Note that the artifact on the boundary of the images $\boldsymbol{x}_t$ is due to the fact that the training loss and evaluation metrics are only calculated on the central 320×320 part of the images, following the previous setting [1, 4] .

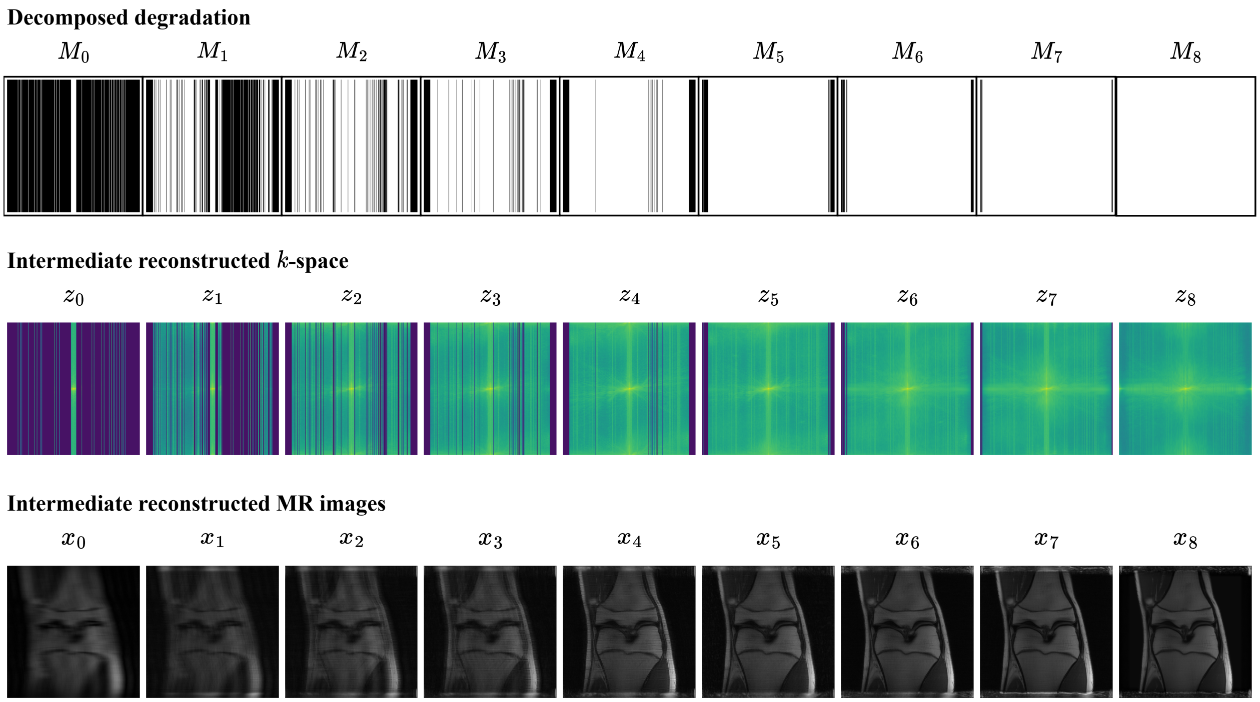

Figure C. Visualization of each intermediate results of decomposed degradation M_t, reconstructed k-space $\boldsymbol{z}_t$ and reconstructed MR images $\boldsymbol{x}_t$, respectively, with total iteration $T = 8$.

D. More Visual Examples

We provide more visual results of $8\times$ accelerated MRI reconstruction on multi-coil fastMRI knee dataset in Figures D&E and Stanford2D FSE dataset in Figures F&G.

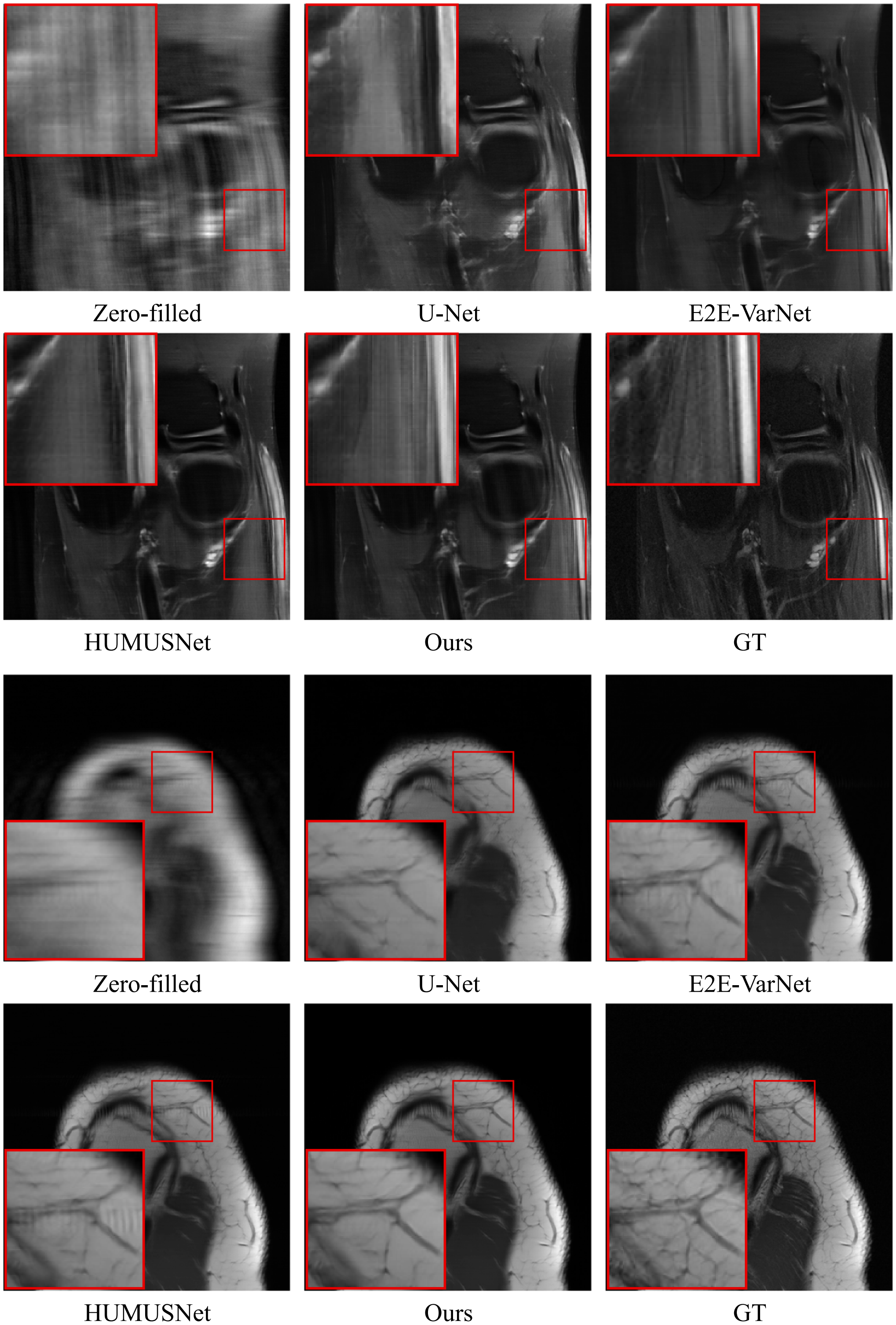

Figure D. Visual examples of $8\times$ accelerated MRI reconstruction on multi-coil fastMRI knee dataset with zero-filled, U-Net [3], E2E-VarNet [4], HUMUSNet [1], ours and ground truth.

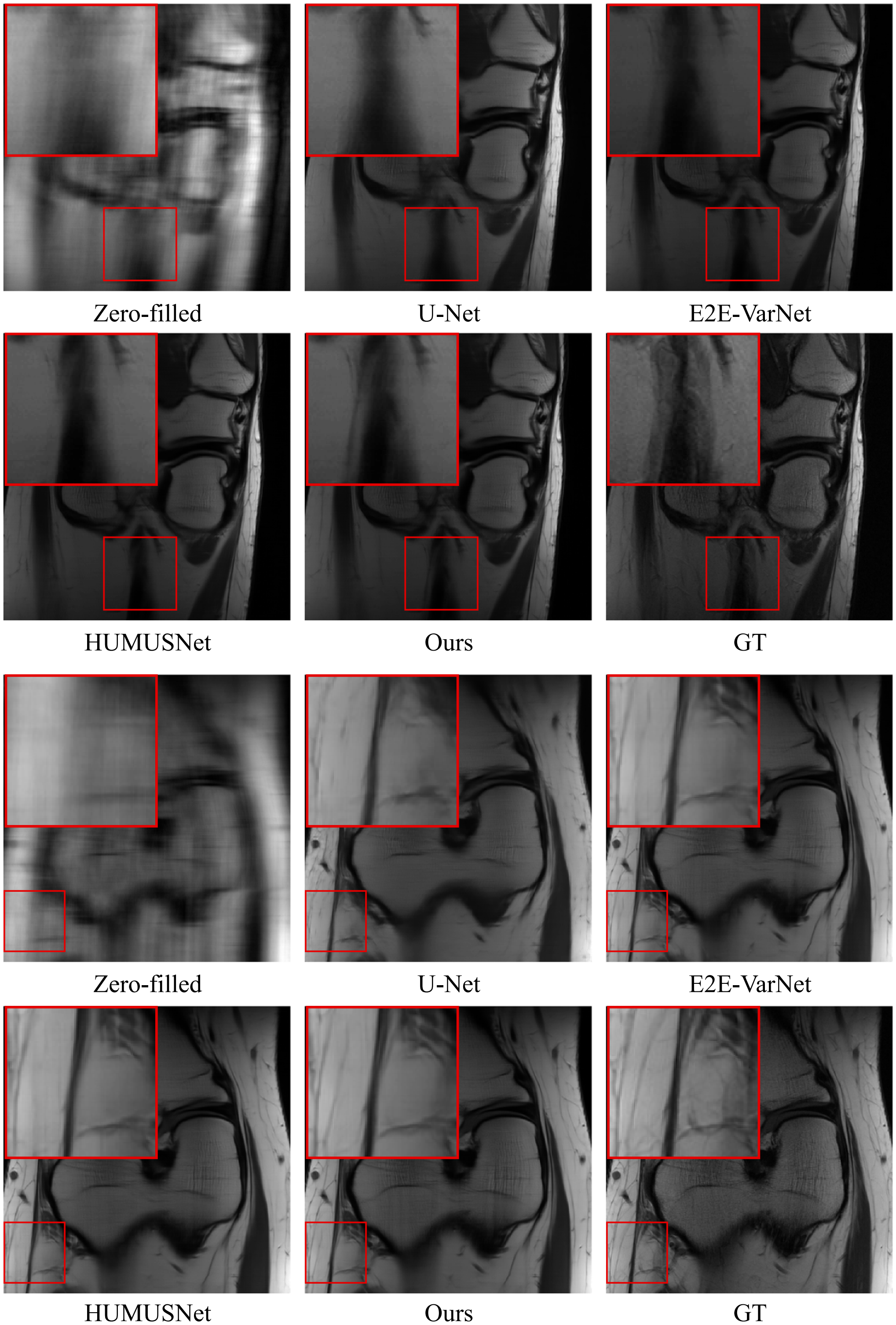

Figure E. Visual examples of 8× accelerated MRI reconstruction on multi-coil fastMRI knee dataset with zero-filled, U-Net [3], E2E-VarNet [4], HUMUSNet [1], ours and ground truth.

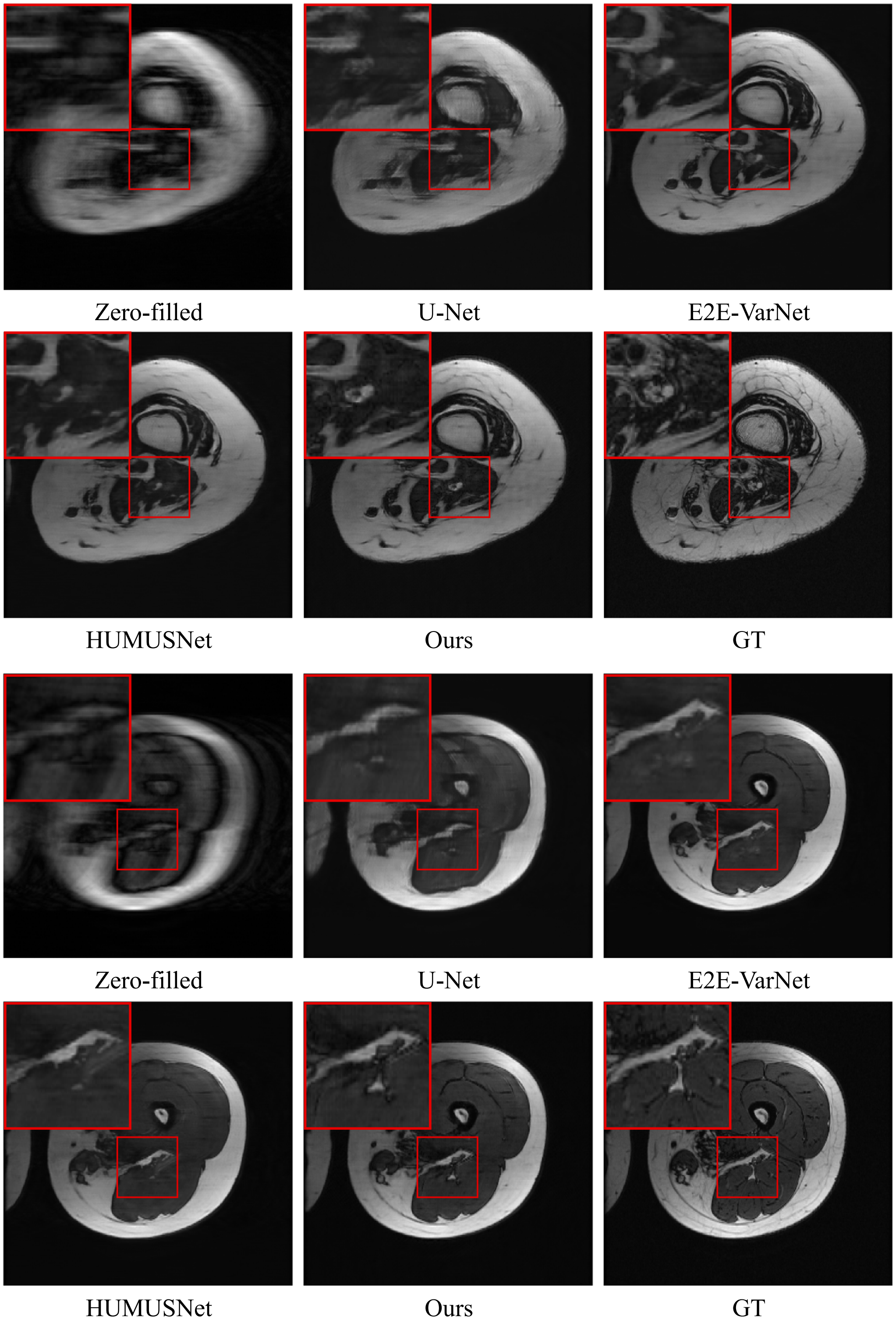

Figure F. Visual examples of $8\times$ accelerated MRI reconstruction on multi-coil Stanford2D FSE dataset with zero-filled, U-Net [3], E2E-VarNet [4], HUMUSNet [1], ours and ground truth.

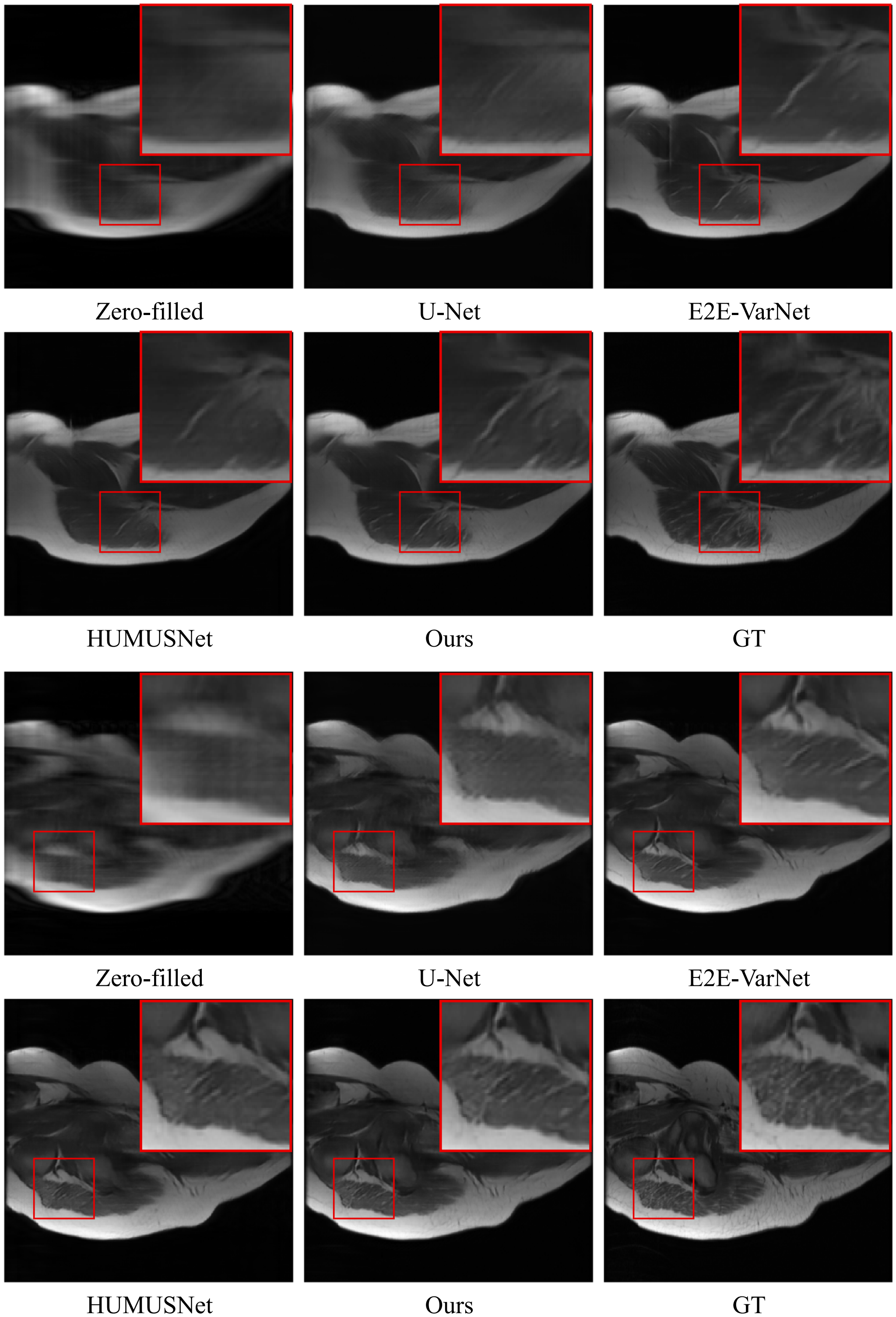

Figure G. Visual examples of $8\times$ accelerated MRI reconstruction on multi-coil Stanford2D FSE dataset with zero-filled, U-Net [3], E2E-VarNet [4], HUMUSNet [1], ours and ground truth.

References

[1] Zalan Fabian, Berk Tinaz, and Mahdi Soltanolkotabi. Humus-net: Hybrid unrolled multi-scale network architecture for accelerated mri reconstruction. *Advances in Neural Information Processing Systems*, 35:25306–25319, 2022. 3, 4, 5, 6, 7

[2] William Peebles and Saining Xie. Scalable diffusion models with transformers. In *Proceedings of the IEEE/CVF International Conference on Computer Vision*, pages 4195–4205, 2023. 2

[3] Olaf Ronneberger, Philipp Fischer, and Thomas Brox. U-net: Convolutional networks for biomedical image segmentation. In *Medical Image Computing and Computer-Assisted Intervention–MICCAI 2015: 18th International Conference, Munich, Germany, October 5-9, 2015, Proceedings, Part III 18*, pages 234–241. Springer, 2015. 4, 5, 6, 7

[4] Anuroop Sriram, Jure Zbontar, Tullie Murrell, Aaron Defazio, C Lawrence Zitnick, Nafissa Yakubova, Florian Knoll, and Patricia Johnson. End-to-end variational networks for accelerated mri reconstruction. In *Medical Image Computing and Computer Assisted Intervention–MICCAI 2020: 23rd International Conference, Lima, Peru, October 4–8, 2020, Proceedings, Part II 23*, pages 64–73. Springer, 2020. 3, 4, 5, 6, 7